

The determination of shock ramp width using the noncoplanar magnetic field component

J. A. Newbury and C. T. Russell

Institute of Geophysics and Planetary Physics, University of California Los Angeles

M. Gedalin

Department of Physics, Ben-Gurion University, Beer-Sheva, Israel

Abstract. We determine a simple expression for the ramp width of a collisionless fast shock, based upon the relationship between the noncoplanar and main magnetic field components. By comparing this predicted width with that measured during a shock observation, the shock velocity can be determined from a single spacecraft. For a range of low-Mach, low- β bow shock observations made by ISEE-1 and -2, ramp widths determined from two-spacecraft comparison and from this noncoplanar component relationship agree within 30%. When two-spacecraft measurements are not available or are inefficient, this technique provides a reasonable scale size estimation for low Mach shocks.

1. Introduction

The determination of spatial scales within the collisionless shock front is a central problem of observational shock physics. Of particular interest is the width of the shock ramp, defined as the main transition layer between upstream and downstream plasmas. However, without spacecraft measurements in a spatial frame of reference, it is impossible to make comparisons between observations and theoretical models.

For bow shock studies, generally one of two methods is applied to transform the time series observed by an in-situ magnetometer into a spatial profile: (1) the comparison of shock observations made by multiple spacecraft with known separations in time and space [e.g., Russell *et al.*, 1982; Farris *et al.*, 1993; Newbury and Russell, 1996], and (2) the comparison of the duration of the shock foot with the foot length predicted by a model based on the motion of specularly reflected ions [e.g., Schopke *et al.*, 1983; Gosling and Thomsen, 1985; Newbury and Russell, 1996]. Both methods assume that the bow shock is stationary and one-dimensional, and each has its own limitations. The first is not reliable when the time delay between spacecraft observations is too large (non-stationarity can affect the results) or too small (relative errors become large). Also, large transverse spacecraft separations with respect to the shock front can introduce error due to the three-dimensional nature of the bow shock. The second method cannot be applied to laminar shocks (shocks observed during low Mach and low β conditions). At such shocks, ion reflection does not play a dominant dissipative role, and no foot structure is observed.

Because of these limitations, it is desirable to have another independent method for measuring shock scale lengths, particularly for laminar shock observations made by a single spacecraft. In this paper, we make use of the noncoplanar component of the magnetic field within the shock ramp in order to estimate a scale size. This scale size is then compared with a variety of low Mach number shock observations made by the ISEE-1 and -2 spacecraft.

2. Theoretical Basis

Within the ramp layer of a fast collisionless shock such as the Earth's bow shock, the magnetic field is observed to rotate out of the coplanarity plane (the plane defined by the shock normal

and the upstream and downstream magnetic field vectors) [Thomsen *et al.*, 1987]. The analytical relation between this noncoplanar component and the main magnetic component of the shock profile was first derived phenomenologically by Jones and Ellison [1987] in an integral form; its approximate nature has been shown observationally [Gosling *et al.*, 1988; Friedman *et al.*, 1990]. Recently, Gedalin [1996a] examined the noncoplanar component using a general two-fluid hydrodynamics approach, and carried out the derivation with only the widely accepted assumptions of shock stationarity, one-dimensionality, and quasi-neutrality. In the coordinate system where N denotes the direction along the shock normal, L is transverse to the shock plane, and M is directed out of the plane, the general expression for the noncoplanar magnetic field component (B_M) is:

$$B_M \left(1 - \frac{B_N^2}{4\pi n m_i v^2}\right) = \frac{c B_N}{4\pi n v e} \frac{d}{dN} B_L - \frac{c}{n v e} \frac{d}{dN} P_{NL}^{(e)} + \frac{B_N}{n m_i v^2} (P_{NM}^{(e)} + P_{NM}^{(i)}) \quad (1)$$

in the limit $m_e \rightarrow 0$, and where v is the N component of the hydrodynamic velocity; $B_N = \text{const}$ and $n v = \text{const}$; and P_{ij} are components of the pressure tensor.

It has been shown by Gedalin and Zilbersher [1995] that the main contribution to P_{NM} is primarily due to the presence of strong ion reflection and the consequent ion gyration. For low Mach number shocks, significant ion reflection is neither expected or observed, and $P_{NM} \ll n_u m_i V_u^2$ [Gedalin, 1996b]. The $P_{LN}^{(e)}$ term is related to the anisotropy of the electron pressure, which is not typically large, especially in a low- β plasma. Dropping these terms, (1) reduces:

$$B_M = \frac{l_W}{(1 - \cos^2 \theta_{BN}/M_A^2)} \frac{dB_L}{dN} \quad (2)$$

where $l_W = c \cos \theta_{BN}/(M_A \omega_{pi})$ (i.e., $k = 1/l_W$ is the wavenumber of a whistler, phase-standing upstream of the ramp), θ_{BN} is the angle between the upstream magnetic field and shock normal, M_A is the Alfvénic Mach number, and c/ω_{pi} is the ion inertial length. $(\cos \theta_{BN}/M_A)^2$ is usually small for quasi-perpendicular shocks, but is included for completeness. Note that (2) is a differential analog of the integral relation developed by Jones and Ellison [1987].

By measuring the slope of the main magnetic field component (dB_L/dt) within a shock ramp observation and relating it to the local noncoplanar component according to (2), one can determine

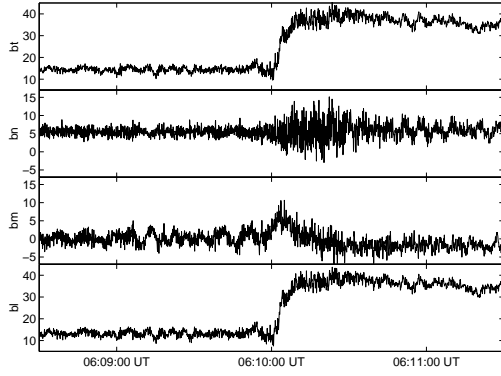


Figure 1. The magnetic profile in the coplanar frame for a laminar shock observed by ISEE-1 on November 26, 1977. $M_A = 2.7$, $\beta = 0.52$, and $\theta_{BN} = 67.0^\circ$.

an independent estimate of the velocity of the shock front. Once the shock velocity is determined, it is then elementary to transform the observed temporal shock profile into a spatial one suitable for comparison with theory, other shock observations, or simulations.

For the observationalist, further difficulties can arise from (2) since it is very sensitive to gradients in the field profile; noise and wave activity associated with a typical bow shock observation can make localized measurements of dB_L/dt difficult. Traditional filtering does not preserve gradients well and can obscure the width of the shock ramp. For laminar shocks, we may apply a simple model which approximates the shock ramp with a hyperbolic tangent:

$$B_L = \frac{(B_u + B_d)}{2} + \frac{(B_d - B_u)}{2} \tanh \frac{3N}{l_r}, \quad (3)$$

where B_u and B_d refer to the L-component of the field upstream and downstream of the shock front, and the coefficient 3 ensures that 90% of the magnetic field variation occurs within the ramp (defined in the region $-l_r/2 < N < l_r/2$). The point where B_M is a maximum is easily identified and will theoretically be located in the middle of the ramp (where $N = 0$). Applying (2) to (3) for $B_{M,max}$, one has a simpler expression for the ramp width:

$$l_r = \frac{3}{2} \frac{l_W}{(1 - \cos^2 \theta_{BN}/M_A^2)} \frac{(B_d - B_u)}{B_{M,max}} \quad (4)$$

This approach requires accurate measurements of B_u and B_d , but is less sensitive to the local B_L gradient than the direct application of (2) to an observed shock profile.

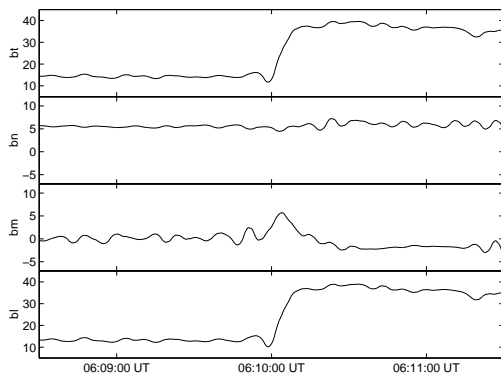


Figure 2. The magnetic profile of the shock, with short period noise removed using a wavelet filter (Daubechies-10 wavelet with the 6 finest scales removed).

3. A Sample Bow Shock

In the present section we apply the proposed method to a quasi-perpendicular collisionless shock crossing that was observed by the ISEE-1 and -2 spacecraft on Nov 26, 1977 at 06:10 UT. Data from the fluxgate magnetometers is filtered to obey the Nyquist criterion and then sampled at the rate of 16 vectors/sec. By averaging over a minute of data upstream and downstream of the shock front and applying the coplanarity theorem, the shock normal is determined, and θ_{BN} is found to be 67° . Figure 1 shows the high-resolution ISEE-1 observation of the magnetic field, rotated into the coplanar frame.

Plasma measurements of the upstream solar wind are obtained by the ISEE-1 and ISEE-3 solar wind experiments, and are used to calculate the following parameters: $c/\omega_{pi} = 58$ km; $M_A = 2.7$ (so that $l_W = 8.3$ km); and electron and ion beta, $\beta_e = 0.36$ and $\beta_i = 0.16$.

In order to remove short wavelength noise while maintaining the gradients within the shock profile, the data was smoothed by applying a discrete wavelet transform (using the Daubechies-10 wavelet) and removing the 6 finest scales [e.g., Chui, 1992; Donoho, 1993]. This corresponds to the removal of features whose scales are shorter than 64 data points ($= 2^6$), which in turn corresponds to ~ 4 sec. averaging for this high resolution data. Although substantial oscillations persist in the upstream and downstream regions, the behavior of B_M and B_L within the ramp is consistent with the theoretical prediction, as seen in Figure 2. Comparison of $B_{M,max}$ with the slope of B_L according to (2) results in a shock velocity estimate of $V_{sh} = 4.4$ km/s. Independently, the shock velocity calculated from the ISEE spacecraft separation is $V_{sh} = 5.7$ km/s (with a separation $L_s = 20$ km along the shock normal and ramp crossing time separation of 3.5 s). The two estimates agree within 25% deviation.

Applying the tanh approximation from equation (3), the ramp width is estimated to be 47.7 ± 7.5 km. Based upon two-spacecraft comparisons, ramp width is found to be 56.7 ± 8.2 km. (The temporal duration of the ISEE-1 ramp observation is approximately 10.25 s) These two estimations of ramp width agree within 20%, which is considered very satisfactory. The error in both calculations is primarily dominated by the uncertainty of the shock normal direction (which affects measurements of the shock velocity, θ_{BN} , the incident solar wind flow, etc.). The normal is determined via the coplanarity assumption: deviations in the measurements of the average upstream and downstream fields propagate through the coplanarity calculations, and are significant (even after the wavelet filtering of the noise on the profile).

4. Application to a Variety of Shocks

In order to estimate the reliability of the method outlined in the previous section, here we compare the results of the proposed approach when applied to a variety of low-Mach shock observations.

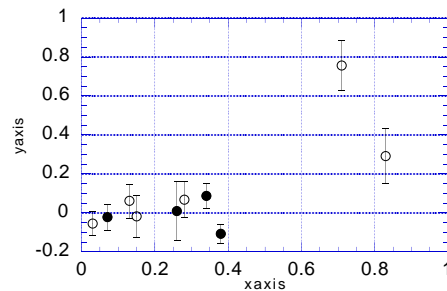


Figure 3. Agreement between the ramp measurement techniques vs. the deviation of B_N during the ramp observation. When B_N remains constant, the noncoplanar technique is most accurate. Open circles indicate supercritical shocks.

Table 1 contains relevant parameters for a selection of shocks observed by the ISEE spacecraft: the Alfvénic Mach number (M_A), ratio of criticality ($R_c \equiv M_{MS}/M_C$, where M_{MS} is the magnetosonic Mach number and M_C is the critical Mach number), θ_{BN} (as determined by coplanarity), total β of the upstream plasma, and measurements of ramp width using the two spacecraft ($l_{r,2SC}$) and based on $B_{M,max}$ ($l_{r,BM}$). These shocks were selected for their low- β , low-Mach, quasi-perpendicular characteristics; in addition, these shocks were observed at times when the ISEE spacecraft configurations were ideal for determining fine spatial scales (i.e., small spatial and temporal separations between observations, and θ_{BN} calculated by coplanarity and via an ellipsoidal bow shock model agree within 10°). Nearly-perpendicular shocks are avoided due to the large errors associated with determining shock normal vectors when $\theta_{BN} > 80^\circ$. (Also, perpendicular shocks may not have the same whistler mode structure as shocks with lower θ_{BN} [Newbury and Russell, 1996; Friedman et al., 1990].) Many of these shocks have been examined previously by Farris et al. [1993].

In Table 1, the ratio of the ramp measurements indicates how well the estimations agree. For eight of the ten shocks in Table 1, agreement between the two techniques is satisfactory (within 30%). Also, they are comparable even when the shock is no longer strictly laminar: several of the shocks listed in Table 1 are slightly supercritical ($R_C > 1$) and are associated with a β that isn't especially low ($\beta > 0.3$).

The shocks observed on 79 Aug 13 and 79 Nov 26 are exceptions: equation (3) does not accurately estimate their ramp widths. The 79 Nov 26 shock is clearly supercritical, and despite the presence of an identifiable non-coplanar component in its ramp, it is expected that ion reflection is a dominant processes at such a shock. The pressure terms in (1) are no longer small, and (2) is not applicable.

The 79 Aug 13 shock is only slightly supercritical, and similar shocks on 77 Nov 26 and 78 Jan 6 agree quite well with (4). This discrepancy can be explained by considering the effects of turbulence and two-dimensional disturbances within the shock profile, as evidenced in the deviations of the B_N component within the ramp layer. Equation (2) assumes that B_N remains constant throughout the shock observation, but in reality this is not always so. Two dimensional disturbances and plasma turbulence on the shock front can obscure the coplanarity rotation. In Table 1, the column labelled $(\delta B_N)/B_{M,max}$ lists the maximum deviation of the B_N component during the shock ramp observation, normalized to the $B_{M,max}$ in the ramp. Within the shock ramp on 79 Aug. 13, fluctuations of B_N are on the order of $B_{M,max}$, resulting in an under-estimated ramp width from (3). Even with the stringent requirements placed on the selection of shocks in Table 1, non-stationarity and turbulence are still a factor which cannot always be ignored. In Figure 3, the ratio of the two ramp measurement techniques are compared with the deviation of B_N during the ramp observation (and normalized to $B_{M,max}$). The shock ramps where the two techniques agree best also have the most constant B_N . However, even a noticeable deviation in B_N can still result in a reasonable estimation of ramp width (for example, the 38% deviation of B_N with respect to B_M for the 78 Aug 27 shock). The open circles in Fig. 3 correspond to supercritical shocks.

For shocks where a foot structure could be discerned, we applied the foot measurement technique outlined by Gosling and Thomsen [1985] ($l_{f,spec}$ in Table 2), and compared it to the foot length measured by the two spacecraft ($l_{f,2SC}$). For the most supercritical shock (79 Nov 26), the foot measurement technique works well and the noncoplanar measurement fails. It is interesting to note that both scale measurement techniques fail for the 79 Aug 13 shock. The remaining observable shock feet agree well with the prediction, generally with uncertainty comparable to that of the noncoplanar technique. One case (80 Sep 6) has a large degree of uncertainty (50%), which is primarily due to the difficulty of identifying precisely where the shock foot begins and ends.

5. Conclusions

We have examined the relationship between the noncoplanar component and gradient of the main magnetic field component within the collisionless shock ramp. By estimating the scale size

of the ramp width based upon this relationship and comparing that length with the temporal duration of a shock ramp observation, we calculate the shock velocity in the spacecraft frame. This enables the observed shock profile to be transformed into a spatial frame, suitable for comparison with other shock observations and with theory.

Assuming that turbulence and any two-dimensional disturbances to the shock front are kept to a minimum, equation (2) should be valid for low-Mach number shocks since the most "dangerous" factor from (1), the non-diagonal ion pressure due to reflected and gyrating ions, is expected to be small. Based upon a sampling of bow shock observations made by ISEE-1 and -2, we conclude that this technique is a satisfactory alternative when two-spacecraft comparisons are not feasible. For slightly-supercritical shocks (where a small foot structure is observed), estimates of scale size based on the noncoplanar-component/ramp-width relationship and based on the specular-ion-reflection/foot-length relationship agree. However, the technique outlined here is most useful for laminar shocks, a variety of shocks for which no independent technique for determining scale size was previously available.

Acknowledgments. The wavelet transform was done using WaveLab package for Matlab. This research was supported by grant 94-00047 from the United States-Israel Binational Science Foundation (BSF), Jerusalem, Israel, and the National Science Foundation under grant ATM 94-13081.

References

- Chui, C.K., *Introduction to Wavelets*, Academic Press, San Diego, 1992.
- Donoho, D., Nonlinear wavelet methods for recovery of signals, densities, and spectra from indirect and noisy data, *Different Perspectives on Wavelets, Proceedings of Symposia in Applied Mathematics*, Vol. 47, I. Daubechies ed. Amer. Math. Soc., Providence, R.I., 1993, pp. 173-205.
- Farris, M.H., C.T. Russell, and M.F. Thomsen, Magnetic structure of the low beta, quasi-perpendicular shock, *J. Geophys. Res.*, 98, 15285, 1993.
- Friedman, M.A., C.T. Russell, J.T. Gosling, and M.F. Thomsen, Noncoplanar component of the magnetic field at low Mach number shocks, *J. Geophys. Res.*, 95, 2441, 1990.
- Gedalin, M., Noncoplanar magnetic field and cross-shock potential in collisionless shock front, *J. Geophys. Res.*, 101, 11153, 1996a.
- Gedalin, M., Transmitted ions and ion heating in nearly-perpendicular low-Mach number shocks, *J. Geophys. Res.*, 101, 15569, 1996b.
- Gedalin, M., and D. Zilbersher, Non-diagonal ion pressure in nearly-perpendicular collisionless shocks, *Geophys. Res. Lett.*, 22, 3279, 1995.
- Gosling, J.T. and M.F. Thomsen, Specularly reflected ions, shock foot thicknesses, and shock velocity determinations in space, *Geophys. Res. Lett.*, 90, 9893, 1985.
- Gosling, J.T., D. Winske, and M.F. Thomsen, Noncoplanar magnetic fields at collisionless shocks: A test of a new approach, *J. Geophys. Res.*, 93, 2735, 1988.
- Jones, F.C., and D.C. Ellison, Noncoplanar magnetic fields, shock potentials, and ion deflection, *J. Geophys. Res.*, 92, 11205, 1987.
- Newbury, J.A. and C.T. Russell, C.T., Observations of a very thin collisionless shock, *Geophys. Res. Lett.*, 23, 781-784, 1996.
- Russell, C.T., M.M. Hoppe, W.A. Livesey, J.T. Gosling and S.J. Bame, ISEE-1 and -2 observations of laminar bow shocks: Velocity and thickness, *Geophys. Res. Lett.*, 9, 1171-1174, 1982.
- Scopke, N., G. Paschmann, S.J. Bame, J.T. Gosling, and C.T. Russell, Evolution of ion distributions across the nearly perpendicular bow shock: Specularly and nonspecularly reflected-gyrating ions, *J. Geophys. Res.*, 88, 6121, 1983.
- Thomsen, M.F., J.T. Gosling, S. J. Bame, K.B. Quest, D. Winske, W. A. Livesey, and C.T. Russell, On the noncoplanarity of the magnetic field within a fast collisionless shock, *J. Geophys. Res.*, 92, 2305, 1987.

Table 1. Shock Parameters and Ramp Measurements

Date, Time [UT]	M_A	R_c	θ_{BN}	β	$\frac{\langle \delta B_N \rangle}{B_{M,\max}}$	$l_{r,BM}$ [km]	$l_{r,2SC}$ [km]	$l_{r,2SC}/l_{r,BM}$
77 Nov 26, 0610	2.73	1.16	67.0°	0.52	0.28	47.7 ± 7.5	56.7 ± 8.2	1.19 ± 0.25
77 Nov 26, 0619	3.07	1.32	69.3°	0.62	0.15	52.3 ± 9.1	50.6 ± 8.6	0.97 ± 0.24
78 Jan 06, 0701	3.21	1.35	56.1°	0.25	0.13	73.6 ± 9.0	88 ± 15	1.19 ± 0.24
78 Aug 27, 2007	2.23	0.85	74.6°	0.16	0.38	127 ± 12	100.3 ± 5.6	0.79 ± 0.09
78 Aug 28, 0009	1.65	0.67	53.5°	0.05	0.26	166 ± 15	197 ± 67	1.18 ± 0.36
79 Aug 13, 1427	3.75	1.40	78.7°	0.10	0.83	34 ± 11	66.7 ± 2.4	1.96 ± 0.64
79 Sep 18, 1029	2.92	1.15	62.3°	0.18	0.03	92 ± 13	83.2 ± 1.5	0.90 ± 0.13
79 Nov 26, 0015	6.00	2.69	67.5°	0.83	0.71	27.1 ± 4.6	154 ± 39	5.7 ± 1.7
80 Sep 06, 1006	2.44	0.98	61.6°	0.17	0.34	71.5 ± 9.3	90.0 ± 6.6	1.26 ± 0.19
80 Dec 19, 1435	1.67	0.62	74.8°	0.04	0.07	102 ± 15	100.0 ± 5.8	0.98 ± 0.15

Table 2. Shock Foot Measurements

Date, Time [UT]	$l_{f,\text{spec}}$ [km]	$l_{f,2SC}$ [km]
78 Jan 06, 0701	224 ± 14	180 ± 28
79 Aug 13, 1427	163 ± 18	66 ± 22
79 Sep 18, 1029	196.9 ± 4.4	166 ± 30
79 Nov 26, 0015	321 ± 22	294 ± 60
80 Sep 06, 1006	180 ± 11	255 ± 90
80 Dec 19, 1435	81.3 ± 3.9	72 ± 21